ASIA TURBOMACHINERY & PUMP SYMPOSIUM
12-15 MARCH 2018
SUNTEC SINGAPORE

EROSION PREDICTION OF GAS TURBINE COMPRESSOR BLADES SUBJECTED TO WATER WASHING PROCESS

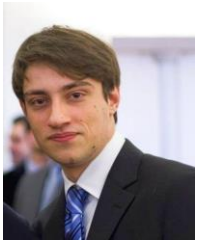

Alessandro Chiariotti
M.Sc.
Sapienza University of Rome
Rome, Italy

Domenico Borello,
Ass. Professor
Sapienza University of Rome
Rome, Italy

Paolo Venturini,
Research Associate
Sapienza University of Rome
Rome, Italy

Salvatore Costagliola,
Engineering Manager
Baker Hughes a GE Company
Florence, Italy

Serena Gabriele,
Systems Engineer
Baker Hughes a GE Company
Florence, Italy

ABSTRACT

Blade fouling is a relevant problem in turbomachinery applications. It affects both compressors and turbines. In the first case, fouling can be generated by the presence of dust, ashes or brackish air (in offshore applications). In turbines, fouling is mainly generated by residual of combustion process. Blade fouling generally leads to a reduction of the performance due to an increase on profile losses. Here we focus on the fouling due to salt deposition on naval/off-shore applications referring to machines that are part of the fleet of gas turbines manufacturers. In such applications, it is common to introduce on-line washing devices aiming at removing fouling from the early stages of the compressors. The water is sprayed upstream of the first rotor, it impacts on the rotor blades and thus dissolving the deposited salt. However, this procedure possibly leads to blade erosion and/or corrosion. A clear comprehension of the erosion mechanism is the main objective of the present work. To this end, we propose an integrated multi-phase CFD tool. The multi-phase flow is analyzed by adopting a one-way coupling, thus assuming water droplets to be drag by the carrier flow without influencing the main flow. The droplets are dispersed and tracked singularly by adopting a Lagrangian approach. As for the erosion, well-known and widely accepted models are used.

The capability of a Lagrangian code, P-Track, developed and validated at the Department of Mechanical & Aerospace Engineering, Sapienza University in Rome, is presented. The code is able to predict the droplets trajectories, as well as to simulate the impact on the solid walls and the erosion mechanism. Simulations were performed using 25 and 100 μm droplet size. Results, expressed in terms of normalized erosion rate, show the erosion patterns and erosive effect of the two size classes. Erosive capacity is proportional to droplet size, and the most eroded part of the blade is the leading edge, which is in qualitative agreement with measurements.

INTRODUCTION

Gas turbines power plants are usually equipped with air filtering systems to reduce the possibility for solid particles to reach the compressor and give rise to fouling, that is the deposition of solid particles on a solid surface (compressor blades and vanes in this case). Compressor fouling is a serious problem for gas turbine plants, since it can be responsible of about 70-85% of their performance degradation (Song et al., 2003). Indeed,

particles (i.e., dirt, dust, salt, etc.) deposition on compressor blades alters the blade shape, distorts the airflow, reduces the mass flow through the compressor, and occasionally the compressor pressure ratio (Jordal et al., 2002). The main effect of compressor fouling is to decrease the power output of the full cycle. Other insidious effects include a reduction of the compressor surge margin (Aker and Saravanamuttoo, 1989), thus provoking a very unstable operation of the whole power plant.

To reduce fouling, compressor periodically undergoes water-washing process in which water and some specific additives are sprayed on the compressor blades to wash them. After washing process, the profile losses due to fouling are reduced. Water washing can be performed on-line or off-line. Differently from the off-line water washing, the on-line water wash is performed at full or partial load and consequently with no production loss. Tests performed in site showed that effectiveness of the standard on-line water washing can be improved by adopting a high flow on-line water washing, thus reducing or eliminating the need to perform the off-line water washing. However, this technique can lead to some drawbacks. When water droplets enter into contact with the blades, especially in the first stage of the compressor, they might erode the blades (Figure 1). Blade shape is modified, thus affecting the performance of both the compressor and the whole plant. Furthermore, erosion can cause the propagation of cracks within the blade up to its failure. Therefore, it is of paramount importance to predict the droplets trajectories and their impact over the blade in order to understand the whole erosion mechanism.

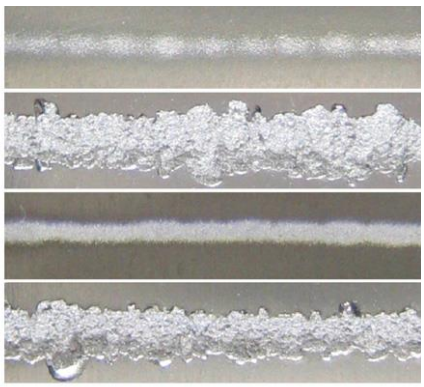

Figure 1. Surface eroded by water droplets (Oka Y.I., Mihara S., Miyata H., 2007).

As said above, water droplet erosion (WDE) is a form of metal erosion caused by the repeated impacts of high-speed droplets over blade surface. This phenomenon gathered importance since the 1970s, starting with studies on the first supersonic aircraft, which presented heavy damage due to the impact with water droplets during rainstorm at high-speed flight. In a 1970 report, drafted for Westinghouse, Heymann tried to identify the main factors driving this phenomenon and to characterize what he called "the mysterious killer of metals". He defined the dynamic of the material removal mechanism, based on the creation and propagation of surface cracks, which leads to the formation of pit cavities inside the material eventually removing metal from the blade. In his experiments, Heymann also discovered that the erosion process starts after a certain period of exposure to droplets impingement. This period was called *incubation period*, later identified as one of the key parameters of the entire erosion process. Moreover, Heymann tried to identify the parameters influencing the resistance to erosion. He discovered that the hardness and strain energy characterize erosion resistance. However, the strain energy is one of the poorest predictors of erosion resistance, when applied to a broad spectrum of materials and thermal treatments. Other experiments aimed at evaluating the influence of the grain size: these experiments showed that the decreasing of the grain size improves the erosion resistance and that material containing finely dispersed small and hard particles in an elastic and ductile matrix are more resistant to erosion.

In conclusion, Heymann identified some key parameters for the WDE, but he was not able to build a comprehensive model that could predict the erosion in a various range of materials and conditions. Since 1970, the erosion was mainly studied by carrying out experimental analysis. Oka *et al.*, (2007), conducted a study focusing on the effective parameters governing the phenomenon. Erosion tests were conducted using a jet apparatus on an aluminum alloy under different pressure condition (10 to 70 MPa) and various standoff distance (30-500 mm). These tests highlighted that jet pressure enhanced the erosion damage, while after a threshold distance the damage depth rate decreased (optimal distance). It was also demonstrated that the incubation period decreased with the increasing of jet-pressure (Figure 2). As for the relation between the impingement velocity and the erosion damage per unit mass of water, it was noted that such relation is represented by an exponential function with an exponent about 6 in the low velocity region (<100 m/s) because the impact force of the water droplets against the material rapidly decreases with the decrease of droplet velocity. At higher velocity region, an exponent of 2 was found because the erosion damage is directly related to the energy of the impinging droplet.

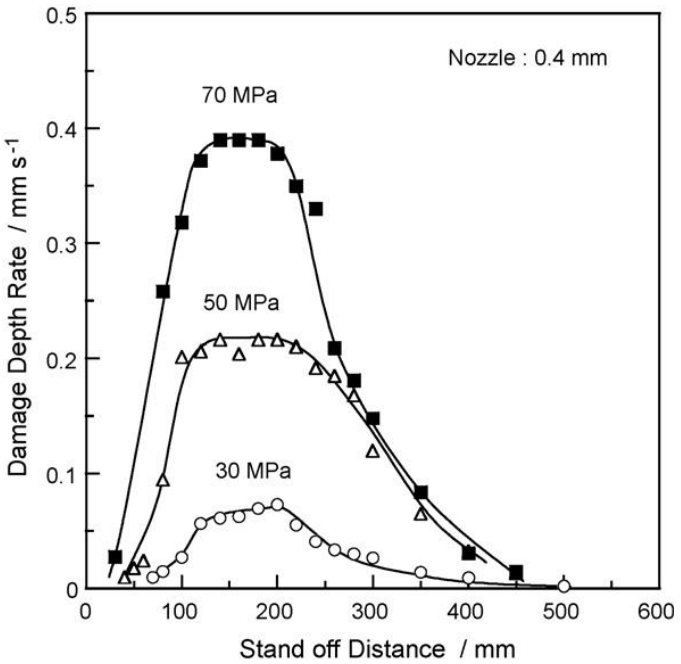

Figure 2. Effective parameters for erosion caused by the water droplet impingement and applications to surface treatment (Heymann, 1970).

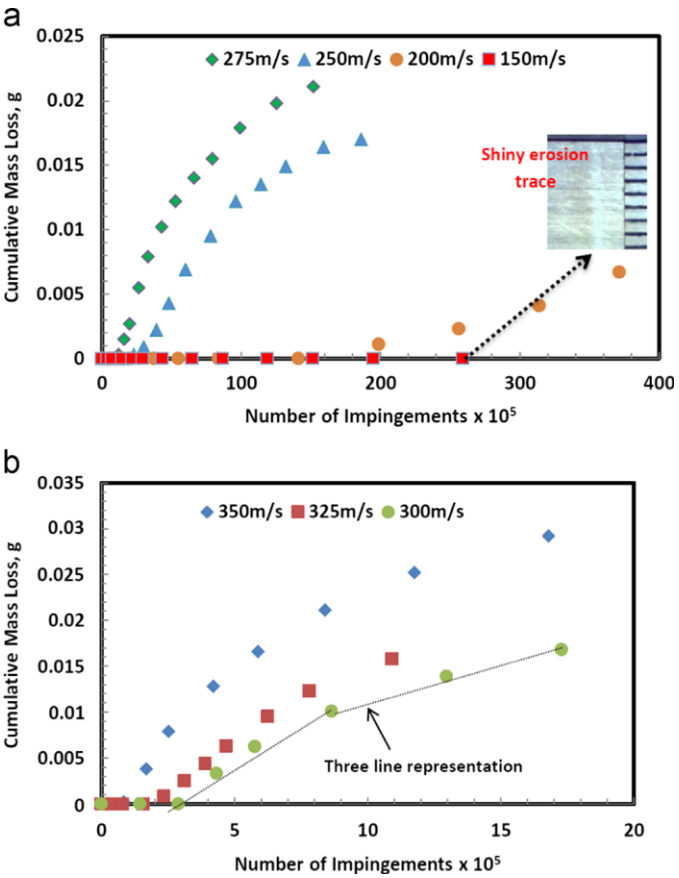

Figure 3. Threshold velocity and erosion damage (Gujba et al., 2016).

Another experimental study was conducted at Concordia University by Gujba *et al.*, (2016). The influence of the impact speed on the WDE behavior between 150 and 300 m/s was investigated and the cumulative mass losses versus the exposure time/number of impingements were studied. A rotating disc test rig, available at Concordia University, was used for studying the WDE behavior. This is a unique testing rig that reaches up to 500 m/s linear speed (equivalent to 20,000 rpm rotational speed). It has a working chamber coupled with a vacuum system, a compressed air driven turbine and a water droplet generating system. The material used was a Ti–6Al–4V alloy, used for gas compressor rotor blades. It was observed that the higher the impact speed, the faster the erosion initiation time and the greater the erosion rate. It was also observed that the erosion rate was related to the impact speed through a log scale with an exponent of 9.9. A threshold velocity range was identified, between 150 and 200 m/s. Above such threshold, it is possible to observe the beginning of the erosion phenomenon, after an exposure time of 840 min, corresponding to 30 million impingements (Figure 3.a). The investigation carefully explored the important stages of the erosion such as the early stage of erosion damage (damage initiation stages) and advanced stages (in Figure 3.b the two stages are shown). These studies showed that the early stages were mainly limited to the formation of micro-cracks, asperities and isolated pits of irregular shape. During the advanced stage, the hydraulic penetration was the most effective cause of material removal. Fatigue striations, walls cracks, sub surface cracks, material folding and upheaving were also observed at the advanced stage.

Sporadically, numerical studies appeared. Li, (2011), investigated the erosion occurred in the inner surface of nuclear power plant bent pipe. One of the cause of WDE erosion is the impact pressure (so called "water-hammer") exerted by the impingement of the droplets drag by the main flow. A single droplet impingement with high velocity on a solid surface was studied using volume of fluid (VOF) approach (Gopala and van Wachem, 2008). The high Reynolds number value implies that the inertia dominates the phenomena and supports the adoption of an inviscid approach for studying the problem. The study showed that the compressibility of the liquid medium plays a dominant role in the evolution of the phenomenon. Both generation and propagation of shock waves were computed by solving the flow governing equations. The numerical results showed that critical pressure is not highest at the center of droplet surface, when the impact occurs, but it is highest behind the contact angle. This finding agreed well with the mathematical analysis and with the theoretical approximation proposed by Heymann, (1970).

Here, we propose the adoption of the model developed by Springer et al., (1974) as a possible approach for studying the effect of WDE on compressor blade during the water-washing process. The model was implemented in the well validated P-Track code developed by some of the authors at Sapienza University of Rome (i.e., Borello *et al.*, 2012, 2013; Venturini *et al.*, 2012; Rispoli *et al.*, 2015; Cardillo *et al.*, 2014, Castorrini *et al.*, 2016). P-Track was properly developed for analyzing: a) two-phase flows using Lagrangian approach, b) impact of particles/droplets over solid surfaces. Here, the code capabilities are demonstrated in a turbomachinery application. In the following paragraphs, the adopted erosion model is described. Then, the carrier flow field is briefly sketched together with the results of the erosion model. Results of numerical simulations are then presented and discussed. Some concluding remarks close this study.

WATER DROPLET EROSION MODEL

A Lagrangian droplet tracking model should firstly track the droplets trajectories from the injection nozzle to the impact on the solid wall, and then estimate the erosion due to the impact of the droplets. Both the aspects are accounted for in P-Track adopting a one-way coupling approach, meaning that droplets motion is affected by the flow but not vice-versa (Sommerfeld *et al.*, 2009).

Despite some WDE models have been proposed even in recent years (see for instance, Lee *et al.*, 2003, Liu *et al.*, 2015), one of the most general and used is the model proposed by Springer *et al.*, (1974). The erosion rate (that is, the amount of eroded mass per impacting droplets) is expressed as a function of the main characteristics of droplets and target material, together with the impact velocity and angle. The model also takes into account the incubation period: the erosion process occurs only after a threshold number of impacts n_i below which no erosion damage takes place. After n_i the erosion process linearly increases with the number of impacts. As a second threshold number of impacts n_f is reached, the erosion process tends to be independent from the successive droplet impacts (Figure 4).

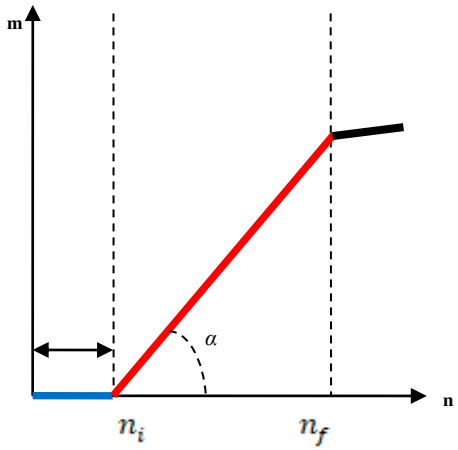

Figure 4. Eroded material as a function of the number of impacted droplets.

The model writes as

$$\begin{cases} m = 0, & if \;\; n < n_i \\ m = \alpha\left(n - n_i\right), & if \;\; n < n_i \\ m = const, & if \;\; n > n_f \end{cases} \qquad (1)$$

being m the eroded mass per number of impacts, and n the number of impacts. The total eroded metal is then given by $\int_{n_i}^{n} m dn$. The value of n_i is a function of the pressure caused by the impact of a droplet on the target material, and the properties of that material. Such value is called water-hammer pressure P:

$$P = \frac{z_R v_{imp} \sin\beta}{1 + z_R / z_C} \qquad (2)$$

In eq. (2), v_{imp} is the impact velocity, β is the impact angle, z is the impedance and subscripts C and R refers to coating and substrate materials, respectively (Springer assumes that the blade is formed of a coating layer and a substrate).

The slope α in eq. (1) is related to n_i by an empirical correlation

$$\alpha = \alpha^* \pi \rho_w d^3 / 6 \qquad (3)$$

where

$$\alpha^* = 0.023\left(\frac{1}{n_i^*}\right)^{0.7}$$

$$n_i^* = 7.0 \cdot 10^{-6} \frac{S_{eff}}{\bar{\sigma}_0} = n_i \frac{\pi d^2}{4}$$

ρ_w is the droplet density (here assumed to be water), S_{eff} is a quantity accounting for the properties of the target material, $\bar{\sigma}_0$ is the mean stress at the impact point, and d is the droplet diameter. For further details see Springer et al., (1974).

PREDICTION OF EROSION

The first step to quantify erosion on GT compressor blades caused by water injection was the CFD prediction of carrier air flow through the compressor from the bell-mouth to the compressor first stage. The droplets trajectories were computed from the spray injection location and then analyzing their spreading and their impact against the first compressor rotor. It must be stressed that the droplets where released from nozzles located in the bell-mouth, then they cross the inlet section and the inlet guide vanes (22 blades) before reaching the compressor first rotor (16 blades). A number of complex circumstances must be addressed in the numerical model. We mention two of them: a) the ratio between the blades number in the IGV and the compressor first stage is incommensurable, then all the stator and rotor blades (plus inlet section) should be meshed (or at least half of them considering 11 and 8 blades respectively); b) the compressor first stage is rotating and then a proper stator/rotor meshing should be considered. To face these problems, we adopted a mixing plane approach. We assumed that a time-average flow solution can be obtained by solving for a time-independent solution and averaging the fluxes in circumferential direction on the interface surface.

Model set up

The adoption of the mixing plane approach allowed to simplify, the creation of the compressor geometry. The computational domain was divided in four parts from the engine inlet to the first compressor rotor. Regions have been sorted as follows: GT inlet, inlet extension, IGV, compressor first stage (Blisk), see Figure 5.

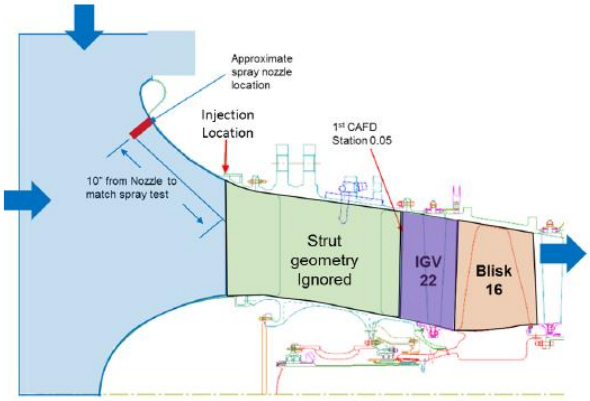

Figure 5. Model Geometry.

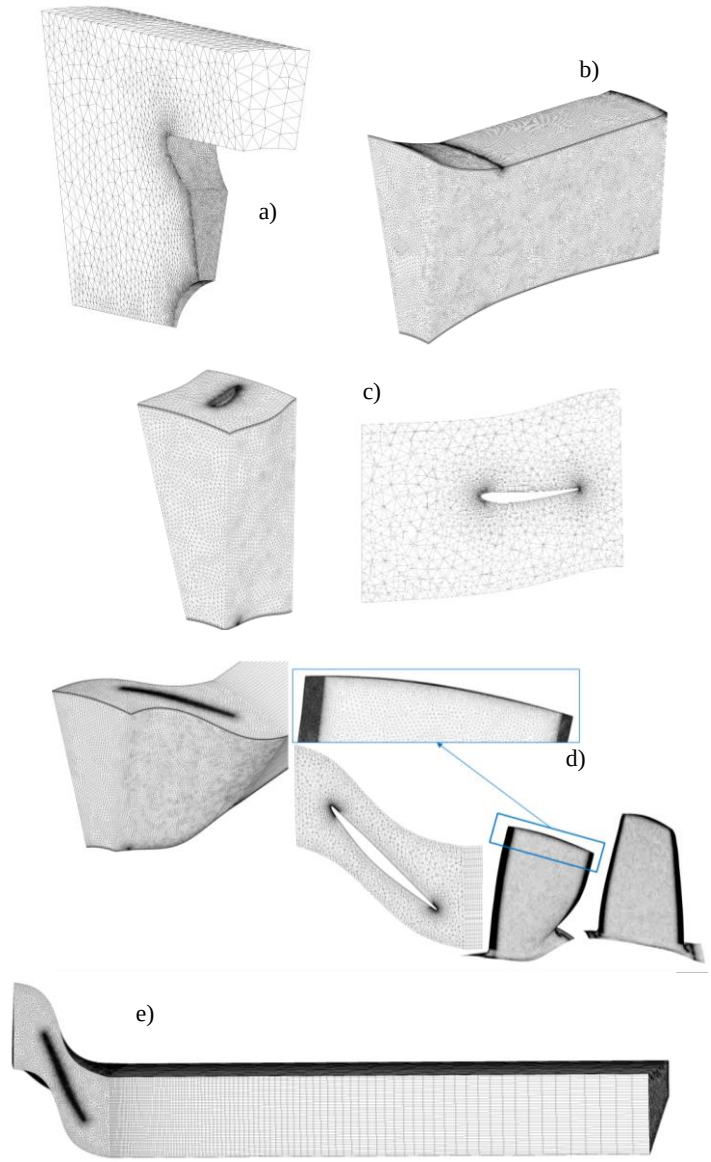

Figure 6. Mesh details: a) Inlet section; b) Bell-mouth and straight duct; c) IGV; d) Compressor first stage; e) Outlet section.

In the figure, the location of the injection nozzle is also indicated. Struts geometry has been ignored as its contribution can be considered negligible to the scope of the analysis. The domain was discretized by using an unstructured grid (Figure 6): tetrahedral cells were used in all the domain except close to the solid walls were prismatic cells were used to improve the prediction of the boundary layer. Wall function was used to model the near-wall boundary layer. The prisms layer was properly adjusted to have a non-dimensional distance of the first cells row 30<y+< 200. Other grid refinements were introduced to ensure the proper resolution of the vane and blade leading and trailing edge curvature, as well as refinements for fillets at the inner or outer Diameter. The total nodes and cells numbers were equal to 10.4M and 3.7M respectively.

The flow field was solved by using ANSYS CFXv16.2.

The turbulent flow governing equations, (continuity, momentum and energy conservation) were solved using Reynolds Averaged Navier Stokes (RANS) closure. Here, the well-established SST Turbulence model (Menter, 2009) was adopted.

Boundary conditions

Total temperature and pressure were fixed at inlet, automatic wall functions were adopted on the solid walls, and outflow boundary conditions were set at the end of the rotor. We point out that to avoid unphysical pressure condition at the outlet, a straight outlet section, 5 hydraulic diameters long, was inserted downstream from the compressor first stage outlet (Figure 6.e). As told before, mixing plane was inserted to model the interaction between the IGV and the compressor first stage regions. It is important to recall that the domain extension in tangential direction is different between stator and rotor. In fact, the stationary portion has an angular extension of about 16°, while the rotating part has an angular extension of 22.5°.

The turbulent flow governing equations, (continuity, momentum and energy conservation) were solved using Reynolds Averaged Navier Stokes (RANS) closure. Here, the well-established SST Turbulence model (Menter, 2009) was adopted. As the volume of water with respect to air is very small, when modeling the droplet tracking, a one-way coupled approach was assumed.

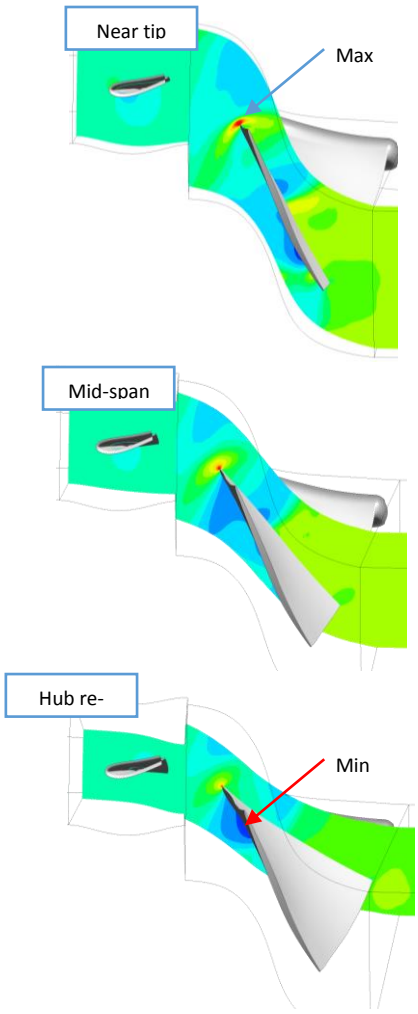

Figure 7. Pressure field at three different span positions.

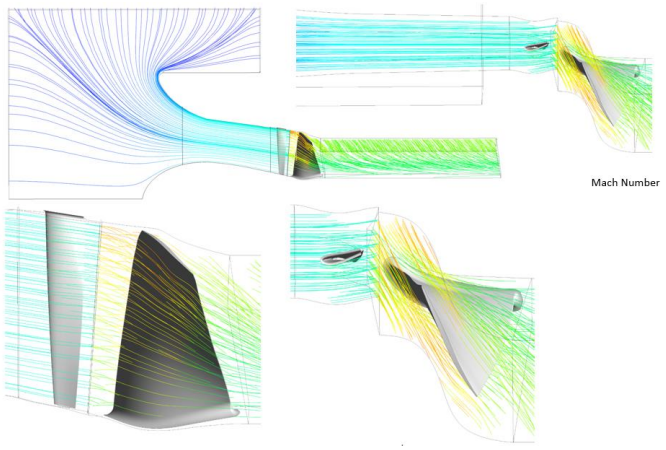

Figure 8. Multi-Stage Model: Flow Field Visualization.

Multi-Stage Model Flow Field Result

Results of simulation are shown in Figures 7-10. At the inlet, stagnant fluid is assumed. When flowing inside the bell-mouth and the IGV region, the maximum Mach number (Ma) increases from about 0 at ambient to about 0.4 at the mixing plane. In the rotating domain, the Ma strongly increases up to a max of about 1.3 that was predicted near the tip of the suction side of the compressor first stage (Figure 8).

In Figure 7, the pressure field at three different span positions, near the tip, near the hub and at mid span, is shown. The coupling between the IGV and compressor first stage required the application of mixing plane. Focusing on the compressor first stage, we notice that in all the planes, the maximum pressure value is measured at the leading edge where static pressure is close to the stagnation one. Maximum value is reached close to the tip where the tangential velocity is maximum. The minimum pressure value is predicted close to the hub where a strong flow acceleration is present.

In Figure 9, the pressure distribution on the compressor first stage blade is shown. As discussed before, the maximum pressure is predicted along the leading edge. On the pressure side, the streamlines are almost parallel. This suggests that secondary motion is almost negligible, except close to the tip, where the streamlines deviation indicates the development of tip-leakage flow. On the suction side, the fluid velocity is generally higher. The flow is subjected to stronger deviation, thus leading to a large flow separation developing close to the hub when moving towards the trailing edge (Borello et al., 2009). It is arguable that on the suction side the flow acceleration and deviation leads to very low number of impacting droplets on the suction side, while the maximum erosion rate should be obtained on the pressure side.

In Figure 10, the turbulent kinetic energy (k) plot is shown. On the suction side, k distribution indicates several phenomena. First, the region of high k close to the leading edge accounts for the rapid acceleration of the flow downstream from the leading edge. Furthermore, close to the tip and mid-chord, the high k value indicates the presence of the tip leakage vortex generated by the pressure difference across the tip gap (Borello et al., 2007). Finally, starting from a region placed around mid-chord and close to the hub, the low turbulence region extending up to the trailing edge and to about mid-span indicated the presence of the large corner separation vortex (Borello et al., 2010). On the pressure side, the k values are generally lower, due to the lower strain associated to a generally slower flow. The only peak is located in the position where the fluid starts to cross the tip gap driven by the pressure difference between pressure and suction surface (tip leakage flow).

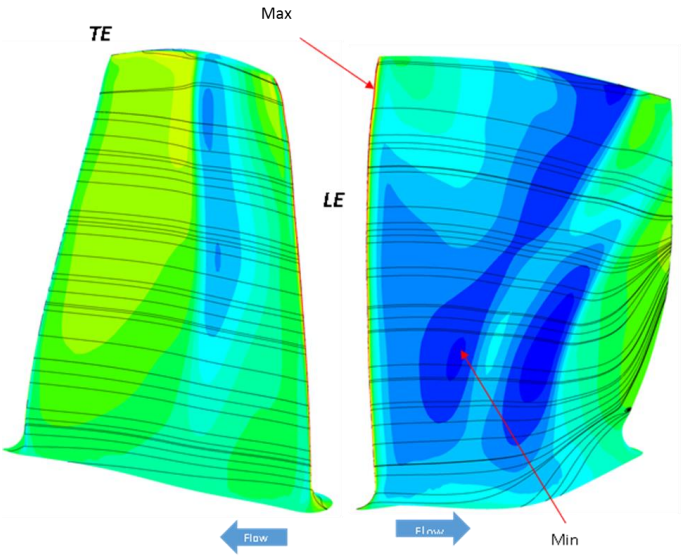

Figure 9. Pressure field in the pressure and the suction side.

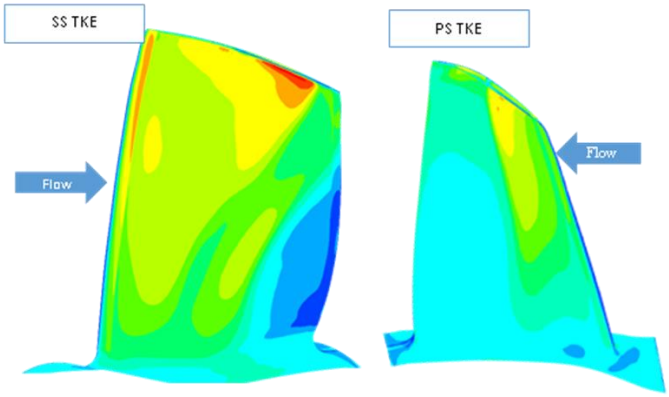

Figure 10. Multi-Stage Model: turbulence kinetic energy.

Erosion

In order to reduce the computational time, a preliminary simulation was performed to individuate the region of the blisk inlet surface where droplets are concentrated. To this end, several droplets were injected from the nozzles mounted on the bell mouth (see Figure 5) and tracked until they reached the blisk inlet surface (Figure 11, red lines). We used this information to simulate WDE on the compressor blade: a large number of water droplets were then released from that region with the same flow velocity. This means that only the central portion of the blade is invested by droplets, as in the actual case. Moreover, in real application droplets size distribution ranges between about 10 and 300 μm, with a maximum injected mass between 90 and 110 μm. Here we simulated two droplets size classes, namely 25 and 100 μm: the latter represents the most relevant size class; the former is chosen in order to study

the effect of droplet inertia on erosion patterns. Indeed, despite the Stokes numbers are larger than unity (Stk=4 for 25 µm droplets, Stk=66 for 100 µm ones), and then inertia is the dominating effect, they differ of about one order of magnitude, thus erosion patterns are expected to show some differences. In Table 1 main characteristics of the simulated droplets are summed up.

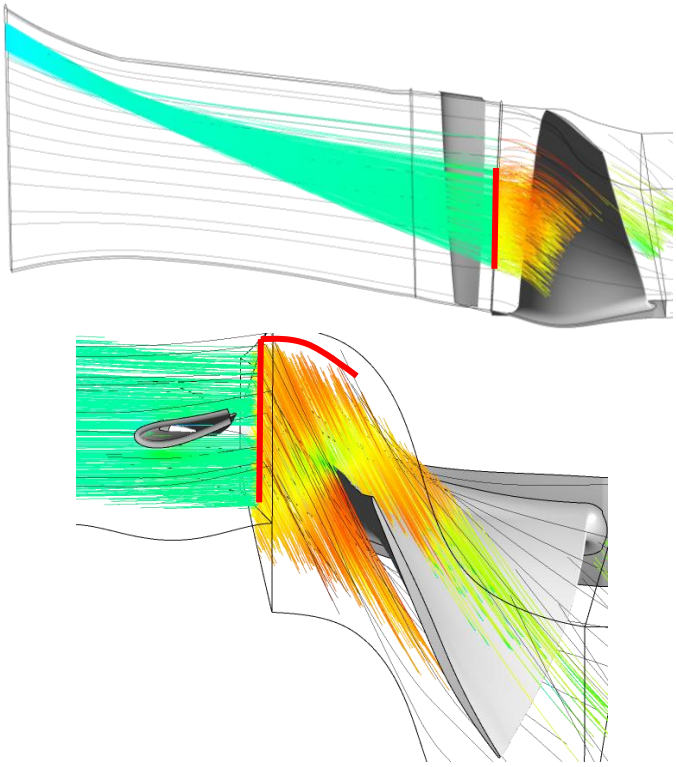

Figure 11. Preliminary simulation: trajectories of the released droplets and droplet inlet region (red lines) in blisk domain for WDE simulation.

Table 1. Main characteristics of the simulated droplets

Size	Inlet vel.	Material	Stk	Simulated
25 µm	Flow	Water	4	>100000
100 µm	Flow	Water	66	>100000

Figures 12 and 13 show the impact positions (colored with impact angle) of both the droplet size classes on pressure and suction sides of the blade. According to what we found in the preliminary simulation, droplets mostly impact the blade on the suction side (see also Figure 11). Only a limited number of impacts are found on the suction side, and all of them are within a narrow region close to the leading edge (Figure 13). Since the Stk number is larger than one for both size classes, droplets have a ballistic behavior, hence their impact angles (Figures 12 and 13) follow the blade swirl. The only difference is at the leading edge, where droplets impact the blade with an angle ranging from 50° to 90°, and this will affect the erosion patterns, as shown further on.

Figure 14 represents the droplets impact points on pressure side colored with impact velocity. As shown in figure (bottom), the 100 µm droplets impact velocities are divided into clear regions, with the higher velocities located after the mid span.

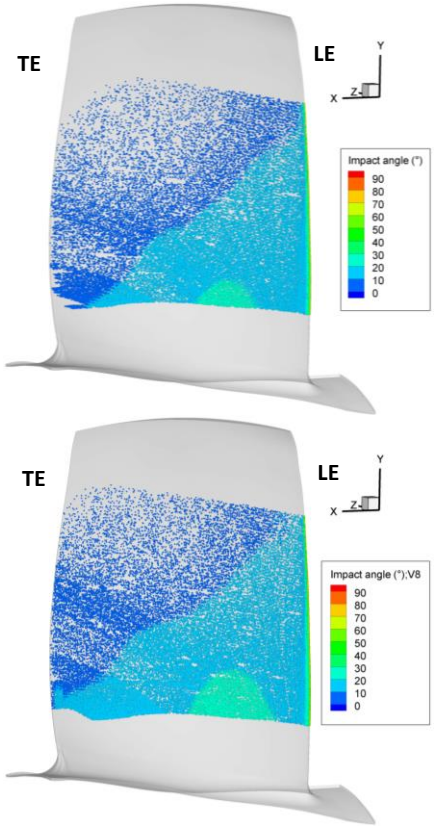

Figure 12. 25 (top) and 100 (bottom) µm droplets impact points on pressure side colored with impact angle (LE: leading edge; TE: Trailing edge).

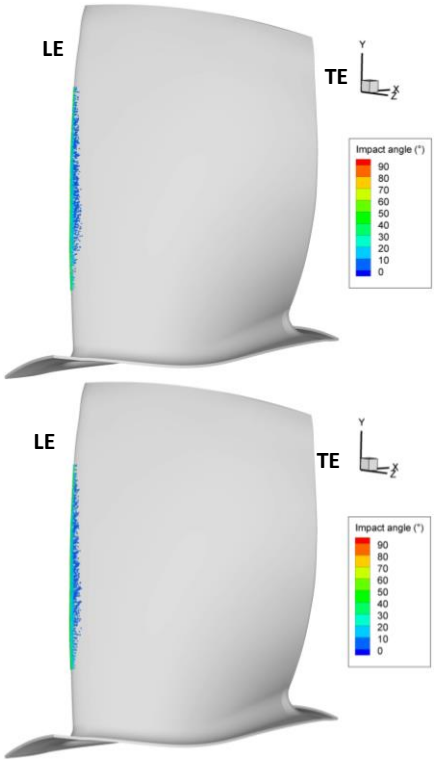

Figure 13. 25 (top) and 100 (bottom) µm droplets impact points on suction side colored with impact angle (LE: leading edge; TE: Trailing edge).

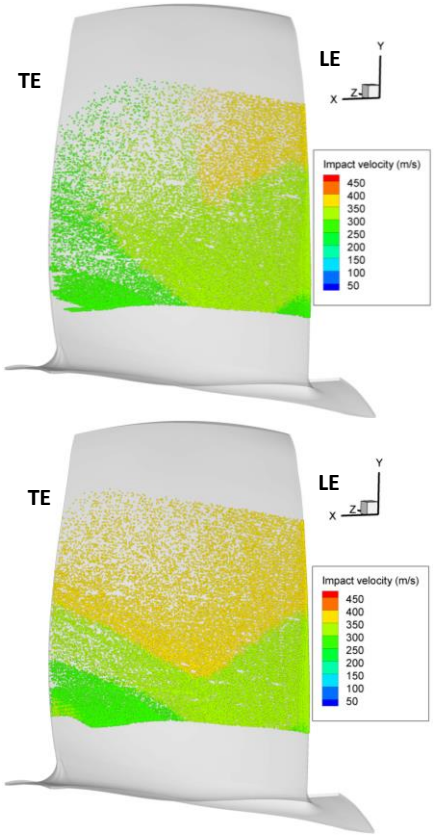

Figure 14. 25 (top) and 100 (bottom) µm droplets impact points on pressure side colored with impact velocity (LE: leading edge; TE: Trailing edge).

A slightly different behavior is found for smaller droplets. Even in this case indeed, the impact velocities are larger after the mid span, but there are divided into less defined regions (Figure 14, top) and having a different spread on the blade. This effect is again due to the different inertia: smaller particles are more reactive to flow variations, and this affects the impact velocity.

Since erosion rate depends on the number of simulated droplets, in order to have results independent from this quantity we compute the normalized erosion rate per unit surface. It has been used two different normalizations: in the first the actual erosion rate is normalized with the simulation maximum value (ER-l), and with the maximum of both simulations (ER-n) in the second one. While ER-l can be used to compare the erosion patterns due to different droplets size classes, ER-n allows to compare their erosive capacity, therefore individuating the most dangerous size range. These two simple quantities are very useful: they can be used in the design process in order to optimize the blade profile, and in the management of water washing operations avoiding the usage droplets in the most erosive size, and helping to plan a proper maintenance.

Figure 15 shows ER-l for both size classes; only pressure side is reported because on the suction side, as already seen, there is no erosion except for the narrow stripe close to the leading edge. As shown, the erosion patterns are very similar. Three main erosion regions can be identified in both cases: one at the leading edge, showing the largest erosion (A) and involving a narrow stripe also on the suction side (A'); another (B) after the leading edge region, toward the trailing edge, in which the erosion rate is smaller than in A; the last region (C) is at the bottom of the blade close to the trailing edge, where a recirculation is present. The rest of the blade invested by droplets shows a very small erosion rate (blue region in Figure 15). Regions named A and A' are similar for both the droplet classes, being narrower toward the tip of the blade (especially in the pressure side) and becoming wider toward the hub. Regions B and C are a bit wider in the case of 25 µm droplets, but thinner, compared to 100 µm one. These differences can be ascribed to the different inertia of the two simulated classes of droplets: smaller ones react faster to flow deviations and this causes a wider dispersion. Despite these slight differences, the erosion patterns are really similar: as all the particles have a Stokes number greater than 1, their strong inertia makes their trajectories not much influenced by the flow field. As a consequence, the droplets impacts are concentrated on the lower side of the blade following more or less a straight trajectory. Erosion mechanism is then consequently concentrated in the lower blade region, even if the larger impact velocities are reordered at the upper part of the blade.

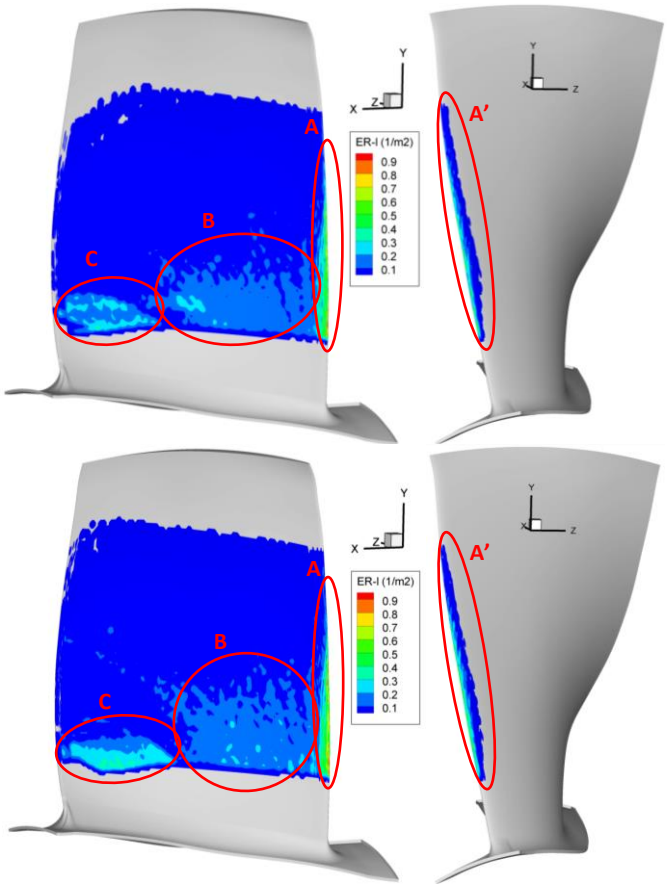

Figure 15. 25 (top) and 100 (bottom) µm droplets normalized erosion rate (ER-l) per unit surface on pressure side (left) and suction side (right). Red ellipses put in evidence the three main eroded regions.

Figure 16 show the normalized erosion rate ER-n on pressure and suction side for both droplets size classes. By comparing the two simulations (Figure 16 top and bottom) it is evident

that larger droplets are extremely more erosive than the smaller ones, as expected. This is due to the impact energy which is proportional to the droplet mass, that is, the larger the droplet mass the larger is its erosive potential. However, erosion also depends on other quantities (i.e., impact angle and velocity), hence the erosion rate is a combination of all these quantities.

The region most exposed to erosion is the leading edge, and this is in good (qualitative) agreement with measurements made on other compressor blades exposed to WDE (Figure 17).

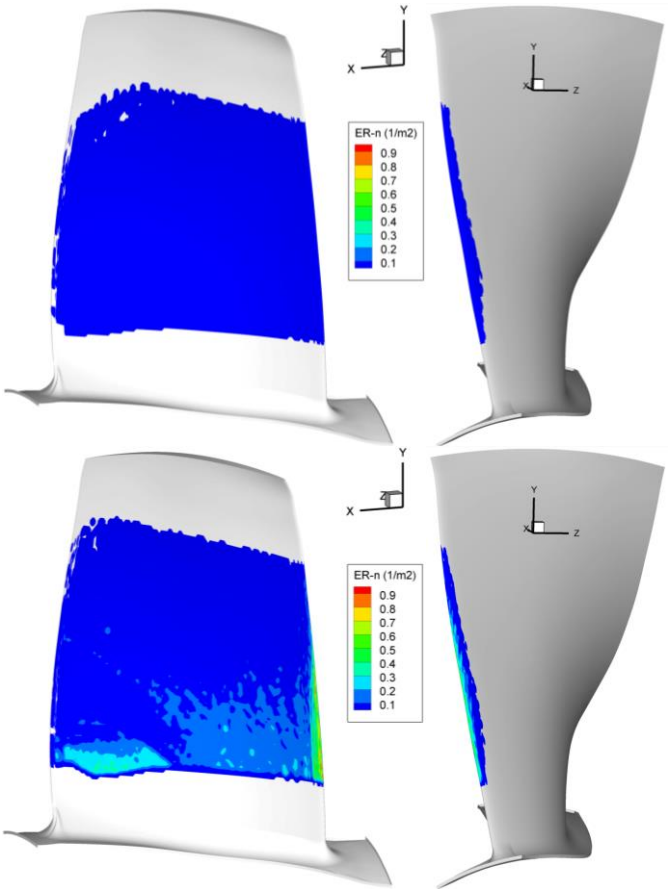

Figure 16. 25 (top) and 100 (bottom) µm droplets normalized erosion rate (ER-n) per unit surface on pressure side (left) and suction side (right).

Figure 17. Compressor blade exposed to WDE process.

In real situations, another aspect should be accounted for, namely the mass of different size droplets actually impacting the blade. In the present simulation, indeed, it has been simulated the same number of droplets for both classes. This was necessary to study the erosion process, the erosive behavior of different droplets, and the most critical regions of the blade. However, if one wants to realistically predict the eroded mass after a given time of exposition to WDE, the computed erosion rate should be scaled according to the actual mass of impinging droplets.

CONCLUSIONS

Erosion is a very complex problem in compressor blades especially when on-line water-washing techniques are adopted. Here a first step study of a GT compressor was carried out focusing on the droplets erosion over compressor first stage pressure surface.

In the present simulation, the erosion due to two different droplets size classes was analyzed. Introducing two different normalized erosion rates, the first normalizing by the simulation maximum erosion (ER-l) and the second normalizing by the maximum of both simulations (ER-n), are used to help the analysis. ER-l is used to study any difference in the erosion patterns of the two size classes. It was found that, even with some slight differences, the erosion patterns are very similar because of the high Stokes number of both the droplet sizes. On the other side, ER-n is used to compare the erosive capacity of different droplets. The simulations showed that, assuming the same number of simulated droplets for both size classes, the erosion is mainly due to the larger one because of their larger impact energy. However, in order to make a prediction, the actual number of droplets for each size classes should be simulated.

Even if this is only a first step of a long term study, it is already clear that it could be very useful since results can provide data that can be used in the design process, in order to optimize the blade profile, and in the management of water washing operations.

NOMENCLATURE

d	Diameter (m)
k	Kinetic Energy (J)
m	Mass eroded per unit area (kg/m2)
*m**	Dimensionless mass loss (-)
Ma	Mach Number (-)
n	Number of drops per unit area (1/m2)
*n**	Number of drops (-)
P	Pressure (Pa)
S	Parameter defined by equation (kg/m2)
Stk	Stokes Number (-)
v	Velocity (m/s)
z	Dynamic Impedance (kg/m2*s)
α	Rate of mass loss (kg)
α*	Dimensionless rate of mass loss (-)

β	Impact angle (rad)
ρ	Density (kg/m3)
$\bar{\sigma}_0$	Mean stress at the impact point (N/m2)

CFD	Computational Fluid Dynamic
GT	Gas Turbine
IGV	Inlet Guide Vane
RANS	Reynolds Averaged Navier-Stokes
VOF	Volume of Fluid
WDE	Water Droplet Erosion

REFERENCES

Agati G., Borello D., Rispoli F., Venturini P., An innovative approach to model temperature influence on particle deposition in gas turbines, GT57997, TurboExpo 2016, Seoul, South Korea, 13-17 June, 2016

Aker G.F. and Saravannamuttoo H.I.H., 1989, Predicting gas turbine performance degradation due to compressor fouling using computer simulation techniques, Journal of Engineering for Gas Turbines and Power, 111 (2), pp. 343-350.

Borello D., Hanjalić K., Rispoli F., 2007, Computation of tip-leakage flow in a linear compressor cascade with a second-moment turbulence closure, Int. J. Heat Fluid Flow, Vol. 28, pp. 587-601.

Borello D., Rispoli F., Hanjalic K., 2009, Large-eddy simulations of tip leakage and secondary flows in an axial compressor cascade using a near-wall turbulence model, Proc. Institution of Mech. Engineers, Pt A – J. Power and Energy, Vol. 223 (A6 SI), pp. 645-655.

Borello, D., Delibra, G., Hanjalić, K. and Rispoli, F., 2010, "Hybrid LES/RANS study of turbulent flow in a low speed linear compressor cascade with moving casing", ASME Turbo EXPO 2010 conference, Glasgow, UK, June 14-18, 2010.

Borello D., Rispoli F., Venturini P., 2012, An integrated particle-tracking impact/adhesion model for the prediction of fouling in a subsonic compressor, Journal of Engineering for Gas Turbine and Power.

Borello D., Venturini P., Rispoli F., Saavedra G.Z. R., 2013, Prediction of multiphase combustion and ash deposition within a biomass furnace. Applied Energy, 101,413-422.

Cardillo L., Corsini A., Delibra G., Rispoli F., Sheard A.G., Venturini P., 2014, Simulation of particle-laden flows in a large centrifugal fan for erosion prediction. Transactions of the ASME Turbo Expo 2014, Dusseldorf, Germany, paper no. GT2014-25865.

Castorrini A., Corsini A., Rispoli F., Venturini P., Takizawa K., Tezduyar T.E., 2016, Computational analysis of wind-turbine blade rain erosion, Computers and Fluids, 141, pp. 175–183.

Gopala, V.R., van Wachem, B.G.M., 2008, Volume of fluid methods for immiscible-fluid and free-surface flows, Chemical Engineering Journal, 141(1-3), pp. 204-221

Gujba A.K., Hackel L., Kevorkov D., Medraj M., 2016, Water droplet erosion behaviour of Ti–6Al–4V and mechanisms of material damage at the early and advanced stages, Wear, 358–359, pp. 109-122

Heymann, F. J., 1970, Erosion by liquids. Machine Design, 10, 118-124.

Jordal K., Assadi M., Genrup M., 2002, Variations in gas-turbine blade life and cost due to compressor fouling – A thermoeconomic approach, Int. J. Appl. Thermodynamics, 5(1), pp. 37-47.

Lee B-E, Riu K-J, Shin S-H, Kwon S-B, 2003, Development of a Water Droplet Erosion Model for Large Steam Turbine Blades, KSME International Journal, 17(1), pp. 114-121.

Li, Ninokata, Mori. 2011. *A numerical study of impact force caused by liquid droplet impingement onto a rigid wall*.

Liu R., Chen K., Chen J., Zhao J., Liang M., 2015, Simulation studies of solid-particle and liquid-drop erosion of NiAl alloy, Simulation, 1, 10001184.

Menter F., 2009, Review of the shear-stress transport turbulence model experience from an industrial perspective, International Journal of Computational Fluid Dynamics, 23(4), pp. 305-316

Oka Y.I., Mihara S., Miyata H., 2007, Effective parameters for erosion caused by water droplet impingement and applications to surface treatment technology, Wear, 263 (1–6), pp. 386-394.

Rispoli F., Delibra G., Venturini P., Corsini A., Saavedra R., T.E. Tezduyar, 2015, Particle tracking and particle–shock interaction in compressible-flow computations with the V-SGS stabilization and Y Zβ shock-capturing, Computational Mechanics, 55, pp. 1201–1209.

Sommerfeld, M., van Wachem, B., & Oliémans, R.. 2009, Dispersed turbulent multi-phase flow. Best practice guidelines. ERCOFTAC, Brussels.

Song W.T., Sohn J.L., Kim T.S., Kim J.H., Ro S.T., 2003, An improved analytic model to pre-dict fouling phenomena in the axial compressor of gas turbine engines, Proc. Of the International Gas Turbines Congress, Tokyo, paper IGTC2003Tokyo TS-095.

Springer G. S., Yang C. I., Larsen P. S., 1974, Analysis of rain erosion of coated materials, Journal of Composite Materials, 8(3), pp. 229-252.

Tabakoff W., Kotwal R., Hamed A., 1979, Erosion study of different materials affected by coal ash particles, Wear, vol. 52, 161–173

Venturini P., Borello D., Hanjalić K., Rispoli F., 2012, Modelling of particle deposition in an environment relevant to solid fuel boilers. Applied Thermal Engineering, 49, pp. 131-138.